Colloid & Polymer Science Colloid Polym Sci 272:1005–1019 (1994)

Microemulsion microstructure and interfacial curvature

R. Strey

Max-Planck-Institut für Biophysikalische Chemie, Göttingen, FRG

Abstract: The typical phase behavior of microemulsion systems undergoing phase inversion is briefly reviewed. As a model system H_2O–n-octane–$C_{12}E_5$ is studied with various experimental techniques. The occurring microstructures are visualized by freeze fracture electron microscopy and the corresponding domain sizes are quantified by small-angle neutron scattering. From the variations of the domain sizes the mean and Gaussian curvatures of the interfacial film with temperature are determined. It is found that the mean interfacial curvature H changes gradually and nearly linearly with temperature from positive (Winsor I) to negative (Winsor II), passing through zero for bicontinuous microemulsions where these contain exactly equal volume fractions of water and oil. There the interfacial tension between bulk water- and oil-rich phases passes through an extreme minimum. Quantitative knowledge of the curvatures permits the measurements of interfacial tensions between the bulk phases to be discussed in terms of the relative contributions of bending energy and entropy of dispersion.

Key words: Microemulsion – microstructure – bending energy – curvature – interfacial tension – elastic modulus

Introduction

Microemulsions are macroscopically homogeneous mixtures of water, oil, and surfactant. On a microscopic level, however, the mixtures are structured into water-rich and oil-rich domains separated by an amphiphilic film. The nature of the microscopic amphiphilic film has been a subject of intensive research, as its properties are essential for microemulsions as a whole. Already in early works Schulman [1], Winsor [2], Prince [3], and others have discussed the various tensions inside the film, an issue discussed in *theoretical* studies of the interfacial stress profile and bending energy [4–20]. The negative stress component of the water/oil interfacial tension is compensated by positive stresses in both the head and tail regions of the amphiphilic molecules in the film. It has been shown that interfacial tension and bending elastic moduli are related to the various moments of the interfacial stress profile. For applying such theories, the state of curvature of the film and its bending moduli are needed.

In this paper, we characterize *experimentally* the interfacial curvature of the film, as it expresses itself in a systematic metamorphosis of the microstructures if a suitable tuning parameter is varied. As such, temperature, pressure, fourth and fifth components can be applied. Since the pioneering work of Winsor [2], it is well-known that the general phase behavior proceeds as shown schematically in Fig. 1: A mixture containing a sufficient amount of surfactant and equal amounts of water and oil may separate into a water-rich microemulsion in equilibrium with an excess oil phase (Winsor I, $\underline{2}$), an oil-rich microemulsion in equilibrium with an excess water phase (Winsor II, $\overline{2}$), or into three phases with a middle-phase microemulsion in simultaneous equilibrium with excess oil and water phases (Winsor III, 3).

Winsor discussed the progression as being driven by a change in the curvature of the amphiphilic film. Winsor worked at constant temperature

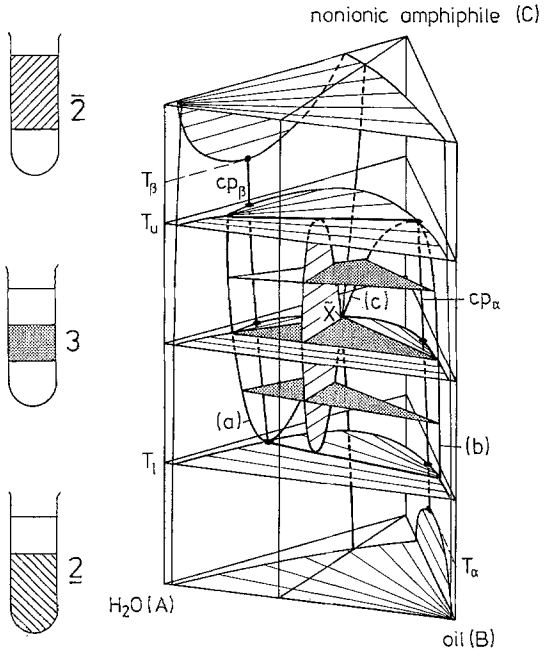

Fig. 1. Schematic phase prism illustrating Winsor I, III, II behavior, denoted here by $\bar{2}, 3, \underline{2}$ respectively. Note that the phase behavior for ternary systems is driven by the convenient parameter temperature.

using *five-component* systems including salt and an ionic surfactant/cosurfactant mixture. Accordingly, he tuned the curvature of the films by the salt concentration and/or the surfactant/co-surfactant ratio.

This kind of formulating microemulsion is still broadly used and has dominated the conception of microemulsions [21–30]. If one does not have the choice of optimal surfactants, it is easier to make microemulsions with five components. However, quantitative measurements and interpretation, in particular of interfacial film properties, are more difficult and inherently uncertain. Interpretation would be facilitated, if one could restrict oneself to the three components really needed: a polar, a non-polar, and an amphiphilic substance. Applying water, oil, and a nonionic surfactant, Shinoda showed in 1967, that the $\underline{2}, 3, \bar{2}$ phase inversion behavior can also be observed in much simpler *ternary* systems [31, 32]. As tuning method, he and his collaborators successfully utilized the advantages of temperature changes [31–36]. In the past decade, Kahlweit et al. [38–43] have systematically studied the phase behavior of such systems as it depends on the nature of the oil and the hydrophilic and hydrophobic parts of the surfactant molecules. The basic features were described already in 1985 in an introductory article [38], which we recommend to newcomers to the field as an entry lecture. The subsequent investigation of the chain length dependence [39] demonstrated that long and short chain surfactants behaved similarly and that there were common properties of the three-phase bodies [40]. It was also shown how the behavior of ionic surfactants differed from nonionic surfactants by the reverse temperature dependence [41, 42]. In a qualitative thermodynamic description the essential features of the phase behavior of microemulsion systems were summarized [43]. One interesting aspect was the empirical finding [40, 43] that the macroscopic interfacial tension between water- and oil-rich bulk phases times the lengthscale in the microemulsion squared always equalled about kT, that is $\sigma_{ab}\xi^2 \approx kT$. Below, we will offer a simple explanation of this fact considering the occurring microstructures and lengthscales. We will argue that interfacial tensions measurements are in fact macroscopic manifestations of the microscopic interfacial stress profile. From the above-mentioned phase diagram studies, we were able to select a suitable ternary system [44] that shows all the interesting features of a microemulsion system, in particular, the microstructure [45, 46] and the striking minimum in interfacial tension between water- and oil-rich phases as one tunes the system through the phase inversion by changing the temperature. In this paper, we present the most interesting features of recently compiled work [47], discuss and document the observed structures, and the associated variations of the curvature of the interfacial film, in order to then interpret measured interfacial tensions in terms of its bending elastic properties. We concentrate mainly on H_2O–n-octane–$C_{12}E_5$ ($C_{12}E_5$: n-dodecyl-pentaethylene glycolether). The techniques which have been previously described in more detail, are small-angle neutron scattering (SANS), freeze fracture electron microscopy (FFEM), electrical conductivity, and spinning drop interfacial tensiometry.

Phase behavior

In studying the phase behavior it has proven useful [48, 38] to perform sections through the

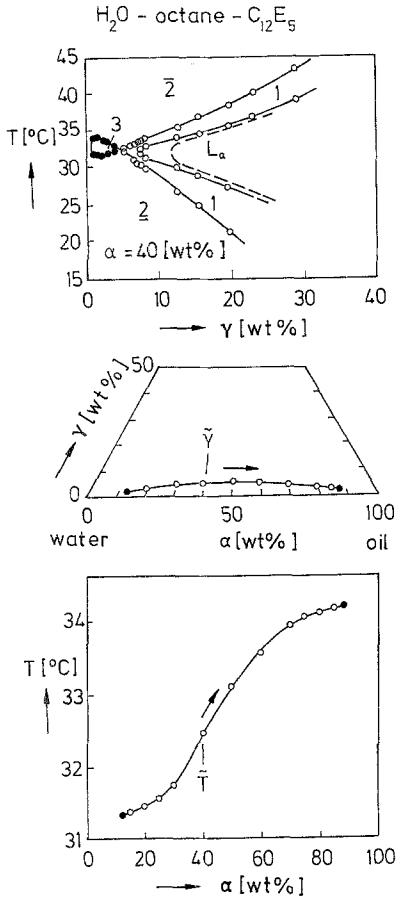

Fig. 2. Section through the phase prism of the H_2O–n-octane–$C_{12}E_5$ (top). The trajectory of the middle phase (denoted by (c) in Fig. 1) is demonstrated by the projections on the bottom (center) and the front face of the phase prism (bottom), respectively.

phase prism at constant water-to-oil ratio expressed by the weight percentage of oil in the mixture of the two and denoted by the symbol α. In Fig. 2 top, we show the section at $\alpha = 40$ wt% which corresponds to about equal volume fractions of water and octane. The most striking feature of such diagrams is the one-phase region (denoted by 1) which, close to the three-phase body, requires the lowest concentration of surfactant (denoted by γ). The point where the three-phase body and the one-phase region meet demarks the composition of the middlephase microemulsion (with surfactant concentration $\tilde{\gamma}$) at that temperature. Also, in this temperature range the lamellar phase extends to very low surfactant concentrations, indicating by its stability that a locally planar amphiphilic film is the most stable configuration, that is, $H = 0$, where the *mean curvature* H is determined by

$$H = \tfrac{1}{2}(c_1 + c_2)\,, \tag{1}$$

with c_1 and c_2 being the principal curvatures. Note that c_i is counted as positive if it tends to enclose the oil and negative if it tends to enclose the water, the latter case corresponding to inverse micelles. For spherical droplet structures, $H = 1/r$, where r is the radius of the droplets. As the temperature is tuned away from the balanced state the microemulsions take up either more oil if temperature is increased, or more water as temperature is decreased. This trend is evident from Fig. 2 center and bottom, which show the trajectories of the middlephase as function of the water/oil ratio or temperature projected onto the bottom plate and front face of the phase prism, respectively. Accordingly, using surfactant concentrations slightly higher than the minimum amount $\tilde{\gamma}$ one-phase microemulsions can be prepared and studied by various techniques (e.g., FFEM [44–47, 49, 50]).

Freeze fracture electron microscopy (FFEM)

Rapid freezing of the microemulsions, followed by fracture and replication of the fracture face yields images of the local structure of the microemulsions. Such images should be considered with care in order not to be misled by artefacts. However, as we have shown first [44–46] (and as has been reproduced [50] by others), images of bicontinuous microemulsions can be obtained in agreement with knowledge on these systems from other techniques. In Fig. 3 center the image of a bicontinuous microemulsion at equal volumes of water and octane is shown. The fracture face of water (amorphously frozen) appears plainly gray, while the fracture face of oils displays a textured appearance. Due to the softer nature of frozen oil, the fracture through the oil is not as planar as through the water domains which fracture glass-like. In some places of the image, one discovers the replication of the hydrocarbon side of the amphiphilic layer. It can be distinguished by a finer texture than that of the oil. From those portions it is evident that the local curvature of the film is a flat one, often with the two principal

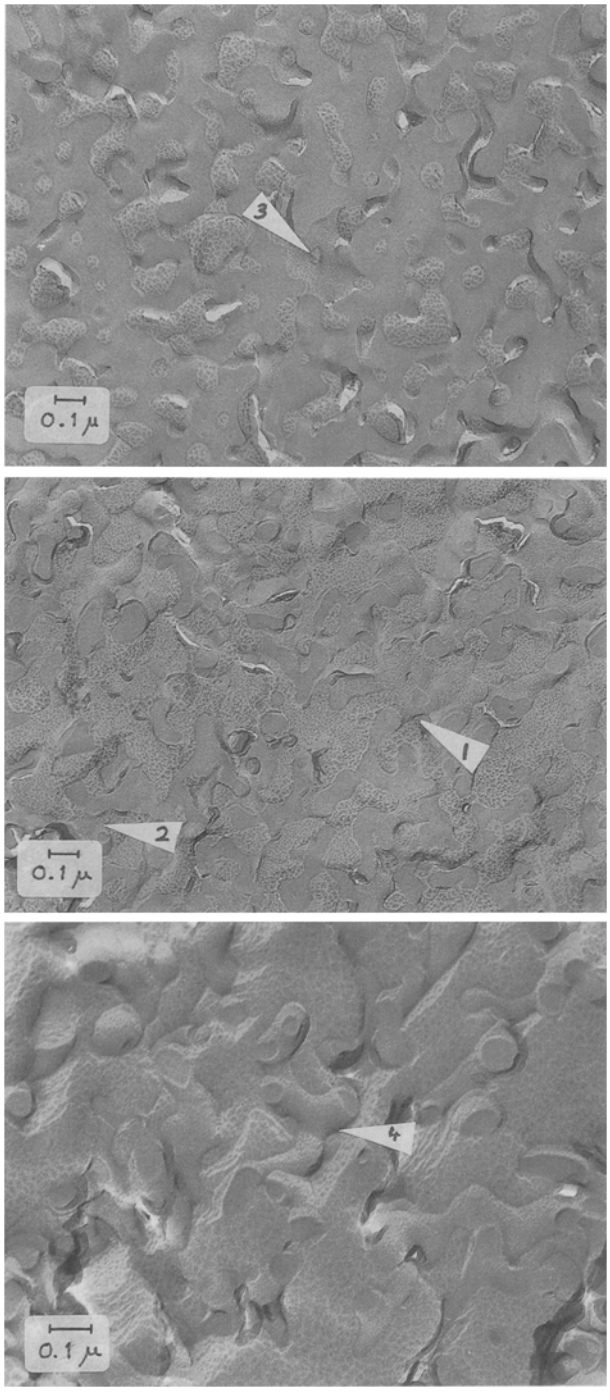

Fig. 3. FFEM images of bicontinuous microemulsions demonstrating the systematic change in microstructure and associated mean curvature of the amphiphilic film. In the center a balanced microemulsion is shown displaying saddle-shaped structures of the film (arrows 1 and 2). As the composition is changed towards more water-rich (top), tubular structures are of oil in water (arrow 3), whereas for more oil-rich microemulsions branched water tubes in oil (arrow 4) can be seen.

radii of curvature of opposite sign; that is, one observes saddle-shaped structures with $K < 0$, where

$$K = c_1 c_2 \tag{2}$$

is called the *Gaussian curvature*. Upon changing the water-to-oil ratio to $\alpha = 30$ wt%, one moves towards the water-rich side. The one-phase microemulsion at $\tilde{\gamma}$ is located at somewhat lower temperature (see Fig. 2 bottom). The image obtained is shown in Fig. 3 top. Compared to the zero-mean curvature image in Fig. 3 center discussed before, now the preferred curvature is towards the oil ($H > 0$), as can be recognized by the frequent occurrence of tubular structures with circular cross-sections. Yet, the oil domains still appear to be connected throughout the solution. Making the corresponding change in composition towards the oil-rich side, that is, going to $\alpha = 60$ wt% with the associated increase in temperature, one finds the image shown in Fig. 3 bottom. Here, the tubular structure is one of interconnected water domains. They can be recognized because they do not break easily, when the oil fracture proceeds around them. One recognizes tubular structures with Y-junctions connecting the cylindrical units. Again circular cross-sections are observed when the fracture occurs normal to the tubule axes. Accordingly, here the mean curvature is $H < 0$. From the sequence of images shown in Fig. 3, we find support for the notion that the mean curvature changes gradually as function of temperature from being positive at low to negative at high temperature. The associated structural change leaves the structures connected. In other words, the structures are bicontinuous, in agreement with NMR- self-diffusion measurements on the same system [44]. The increasing absolute value of the curvature can be traced towards the aqueous and the oleic corners of the phase diagrams along the trajectory of the middle phase. There the structures become increasingly thinner, until at temperatures below T_l and above T_u (defined in Fig. 1) microemulsion droplets of oil in water and water in oil, respectively, are formed.

In order to obtain images of oil in water droplet dispersions, we have developed a technique where water is replaced by water/glycerol mixtures [47]. The equivalent phase sequence as with temperature in the ternary mixtures discussed above can be obtained. Figure 4 demonstrates the phase

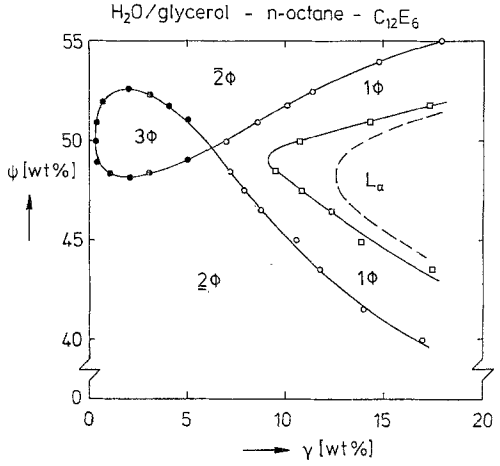

Fig. 4. Phase behavior of pseudo-ternary system (H_2O/glycerol)–n-octane–$C_{12}E_6$ at T = 20.0 °C for volume ratio of polar/nonpolar solvents of unity. Note that the tuning parameter is here the glycerol content ψ in the water/glycerol mixture.

behavior comparable to Fig. 2 top, but here the glycerol weight percentage in the mixture of the two is used to tune the phase behavior of this quaternary system at 20 °C. Using the more hydrophilic $C_{12}E_6$, one can add up to $\psi = 60$ wt% of glycerol, making the aqueous subphase a factor of 10 more viscous and preventing the sensitive droplets from being displaced or destroyed during the freezing process. Figure 5 shows the images of two oil-in-water microemulsions obtained by phase separation of samples of $\alpha = 40$ wt% at $\gamma = 3$ wt% into aqueous microemulsions in equilibrium with excess oil. In Fig. 5 top, we show the result for $\psi = 45$ wt%, and in Fig. 5 bottom for $\psi = 40$ wt%. As can be seen, the droplets become smaller as one moves away from the three-phase regime. It can also be seen that the droplets are quite monodisperse and are randomly distributed throughout the solution.

A schematic representation of the microstructure at equal volume fractions of water and oil as it evolves as function of surfactant concentration is shown in Fig. 6. Figure 6 is based on observations by SANS [52], SAXS [53, 54], NMR-self-diffusion [44, 49, 55] and FFEM [44–46] investigations, and it has recently been applied to and confirmed by a five-component ionic microemulsion system [51]. As the surfactant concentration increases the structures become smaller, because the total area of the internal interface increases,

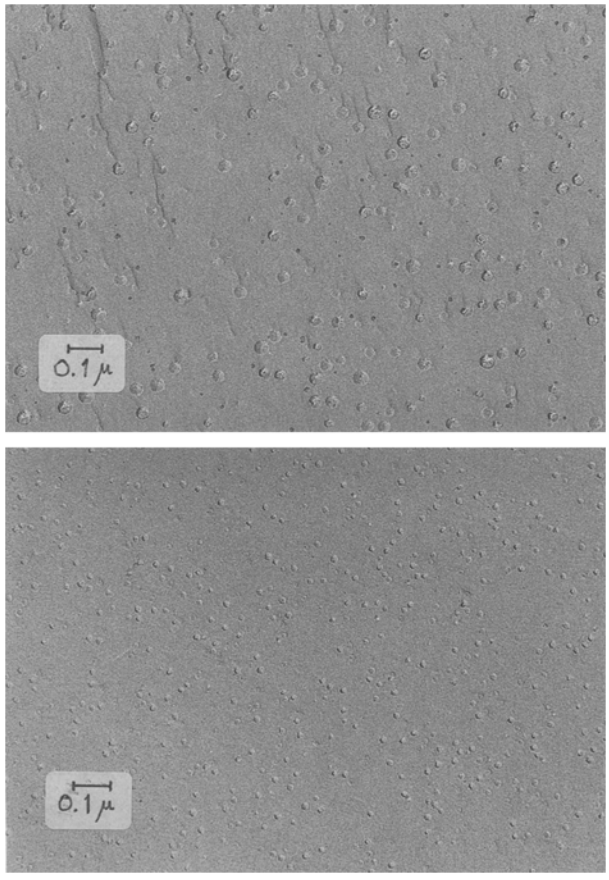

Fig. 5. Microemulsion droplets of the o/w type in the (H_2O/glycerol)–n-octane–$C_{12}E_6$ system. Top, $\psi = 45$ wt%; bottom, $\psi = 40$ wt%. Note the random distribution and small polydispersity.

consistent with the observation that with decreasing droplet size one moves temperaturewise further away from the three-phase regime. At high surfactant concentrations the lamellar phase is observed with a zero-curvature structure ($\langle H \rangle = 0, \langle K \rangle = 0$), whereas near the three-phase region the bicontinuous structure with zero-mean curvature is observed ($\langle H \rangle = 0, \langle K \rangle < 0$). Accordingly, a *gradual* change in the mean and Gaussian interfacial curvature with temperature and composition is the overall observation.

Small-angle neutron scattering (SANS)

The quantitative determination of droplet sizes can be done by SANS provided certain provisions

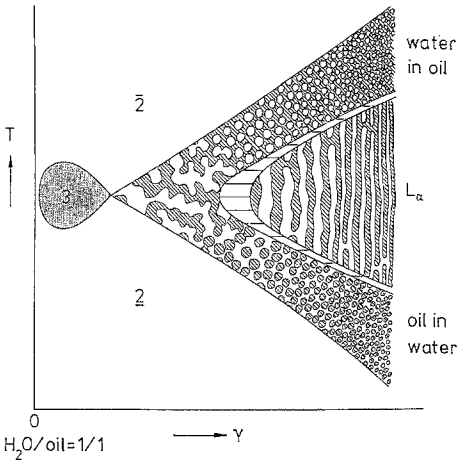

Fig. 6. Schematic representation of occurring structures and their variation with temperature and surfactant concentration.

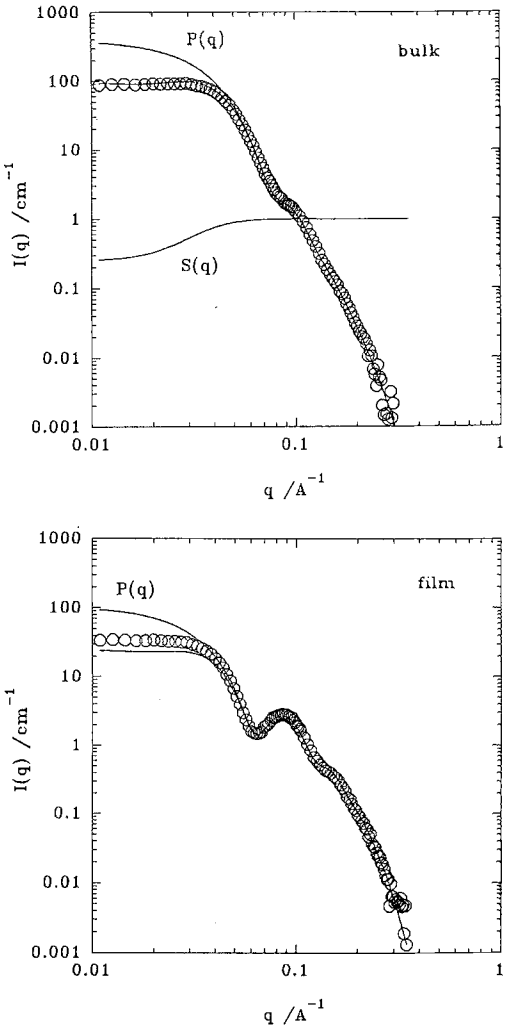

Fig. 7. SANS spectra of o/w microemulsion in bulk (top) and film (bottom) contrast, respectively. Note steep decay at large q indicating a diffuse scattering length density profile.

are taken. As is well-known, the scattering patterns of droplet dispersions are dominated by inter- and intraparticle structure factors. Working in dilute solutions the interparticle structure factor can be made a smoothly varying function, so that the scattering intensity $I(q)$ mainly reflects the particle form factor $P(q)$. With respect to the form factor, SANS offers the useful feature that scattering from certain portions of the particle can be enhanced. For microemulsions the amphiphilic film displays a distinct contrast, if water and oil scattering length densities are matched. We have measured an extensive set of spectra [56] in order to be able to evaluate neutron spin echo experiments on the same system [57, 58]. The existence of a measuring signal of this dynamic technique alone suggests that the droplets have to be conceived as fluctuating objects. Figure 7 shows the static spectra for an oil in water droplet microemulsion in bulk and film contrast ($\phi_b = 0.0506$ and $\phi_s = 0.0759$, measured with D17 at ILL in Grenoble). Evidently, the bulk spectra are less informative than are the film spectra, so that we will only discuss the latter here. Film spectra allow a precise determination of particle radius and polydispersity. The large q part of the scattering intensity in film contrast of spherical droplets can be described by

$$P(q) = 4\pi\phi_s \frac{v_s}{a_s} \frac{(\Delta\rho)^2}{r_0^2 q^2} e^{-q^2t^2} \cdot (f_1 + f_2) \qquad (3)$$

$$f_1 = \frac{1}{2} q^2 t^4 (1 + \cos 2qr_0 e^{-2\sigma^2 q^2}) + qt^2 (r_0 \sin 2qr_0 + 2q\sigma^2 \cos 2qr_0) e^{-2\sigma^2 q^2}$$

$$f_2 = \frac{1}{2} (r_0^2 + \sigma^2 - r_0^2 \cos 2qr_0 e^{-2\sigma^2 q^2} + \sigma^2 \cos 2qr_0 (4\sigma^2 q^2 - 1) e^{-2\sigma^2 q^2}) .$$

This relation is derived by assuming that the interfacial film is penetrated by solvent giving rise to a Gaussian scattering length density profile, similarly to the film scattering from flat structures in bicontinuous microemulsions studied before

[52]. Furthermore, a Gaussian distribution around the mean radius r_0 with variance σ is assumed. In the formula (Eq. (3)) the contrast $\Delta\rho$, the surfactant volume v_s, its interfacial area per molecule a_s, its volume fraction ϕ_s are known quantities from other measurements. Therefore, Eq. (3) describes the large-q part of $I(q)$ on an absolute scale, where $P(q) = N \cdot P_1(q)$ with P_1 being the single particle form factor and the number density of droplets N is calculated from the known amount of the components. Considering for a moment the bulk spectrum in Fig. 7, one observes that the scattering intensity decays steeper than expected from Porod's law (q^{-4}). The analogous expression for the film contrast described by Eq. (3) predicts a steeper decay as q^{-2}, in both cases as a result of the diffuseness of the interface. The diffuseness parameter t turns out to be about 6–7 Å as in the previous study on bicontinuous microemulsions [52]. From Fig. 7 it is also evident that the low q part is influenced by the interparticle structure factor $S(q)$, while $S(q) \to 1$ for large q. It should be noted that the scattering spectra from a droplet microemulsion appear smeared for several reasons. First, there is broadening by the wave length distribution ($\Delta\lambda/\lambda = 0.1$) and resolution limitations due to the pixel size of the detector and the beam divergence. Second, one might anticipate a natural polydispersity and deformations from the spherical shape. For all these reasons, which are difficult to separate from each other, the polydispersity obtained from fitting Eq. (3) to the experimental curves should be considered as an upper bound. One finds, however, that the mean radius r_0 is much less affected and is easily found from the characteristic dip in the scattering pattern being a remnant of the first minimum of the Bessel function involved. The mean radius can therefore be used as a rather accurate measure for the mean curvature $\langle H \rangle = 1/r_0$ which is the quantity we want to extract from the scattering spectra in the context of the present paper.

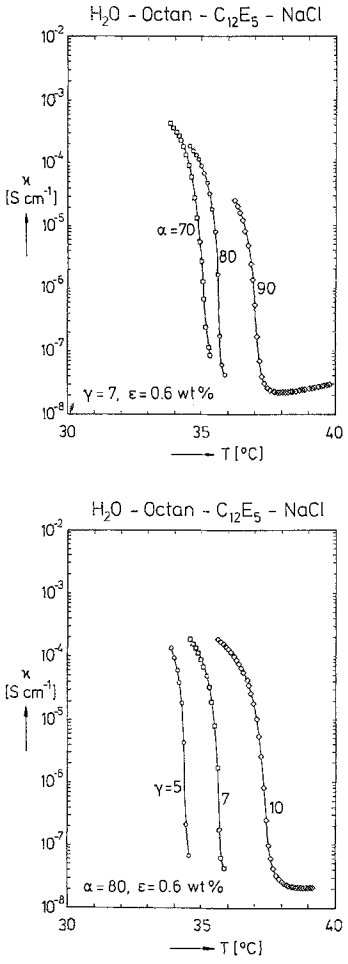

Fig. 8. Electrical conductivity versus temperature of oil-rich microemulsions. Note the systematic trend of the inflection (percolation) point towards higher temperature as the droplets become smaller either with increasing surfactant concentration or oil content.

Electrical conductivity

It was earlier noticed that, when microemulsions are driven through phase inversion, a characteristic jump in the electrical conductivity of the stirred emulsions is observed [61]. This is an important and technically useful observation for emulsions being formulated with unknown or difficult to control ingredients, e.g., as in reaction vessels. A related phenomenon studied mainly in ionic microemulsions [62–64] can be observed in oil-rich one-phase microemulsions as function of the tuning parameter. It has been discussed in terms of stirred percolation [65]. In Fig. 8, we show the effect for the H_2O–n-octane–$C_{12}E_5$ system studied here. Note that the relatively small amount of $\varepsilon = 0.6$ wt % NaCl added to the water in order to have a well-defined ionic strength only negligibly influences the phase behavior. Without entering a detailed analysis in terms of

percolation, which is admittedly tempting, we want to emphasize that within a narrow temperature interval the conductivity drops from very high values to low ones. This can be understood as a transition from a connected, water-continuous structure to an isolated droplet structure. The droplets form at the high-temperature end of the one-phase region (near the phase boundary $\bar{2}$), where the characteristic SANS spectra in film contrast prove their droplet nature. The droplet radii have quantitatively been determined by SANS. The branched tubular nature of the connected structure at the low-temperature end has been verified for the $\alpha = 80$ wt% sample previously by FFEM [44]. The percolation temperature T_p, roughly the inflection point, at which the structures disconnect can be traced as function of α and γ. T_p increases with increasing α and increasing γ. With both parameters the droplet size decreases, that is the curvature of the amphiphilic film of the water droplets increases. Decreasing γ (further than in Fig. 8 bottom), one can trace the percolation temperature towards the body of heterogeneous phases. There, one observes that the temperature of intersection is located close to T_u.

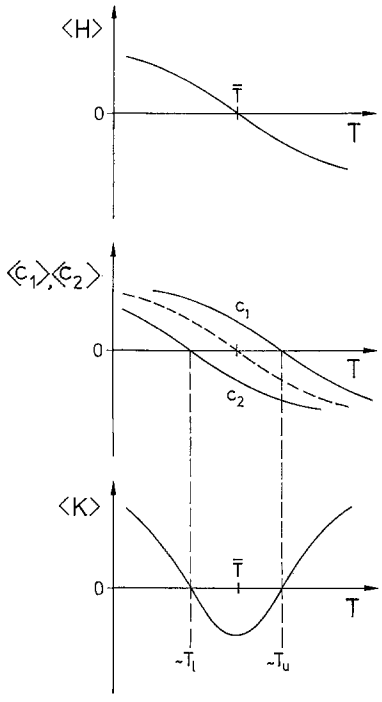

Fig. 9. Principal trends in microemulsion curvatures with temperature. Mean curvature (top), mean curvature (dashed line) decomposed into the two principal curvatures (center) and Gaussian curvature (bottom).

Interfacial curvature

From the evidence given above and from the references mentioned, we arrive at the notion that the mean interfacial curvature of the nonionic microemulsions studied decreases steadily with increasing temperature. Accordingly, one might assume that to *first order* the mean curvature H starts from zero for $\bar{T}$ and varies as shown schematically in Fig. 9 top. Here, we also note that for very high and low temperatures the microemulsion droplets should approach the sizes expected for reversed and normal micelles, respectively. That is, H should level off at both high and low temperatures towards $H_m = 0.06$. Indications for this might be seen for the highest and lowest points in Fig. 10. From the non-zero value and the opposite sign of c_1 and c_2 near $\bar{T}$ and the nearly equal positive value of the c_i for low, and the nearly equal and negative value for high temperatures, one might expect that H is composed of c_1 and c_2 having the same slope as H, but being displaced by a certain margin towards high and low temperature, such that c_1 passes through zero near T_u while c_2 passes through zero near T_l. Note that for cylindrical structures one of the principal curvatures vanishes. The former trend is supported by the tubular, that is, locally cylindrical water domains close to T_u observed by FFEM and concluded from conductivity. Whereas the latter is supported by NMR-self-diffusion studies on the aqueous side on this [44] and related systems [55]. The principal trends in the c_i are shown schematically in Fig. 9 center, which then add to yield the mean curvature shown as a dashed line. Figure 9 bottom shows the resulting Gaussian curvature $K = c_1 c_2$ being positive for the droplet regimes and being negative in the intermediate range where bicontinuous microemulsions occur.

Figure 10 shows the quantitative evaluation of the mean curvature as it is obtained from SANS and FFEM observations. While from SANS we obtain $\langle H \rangle = 1/\langle r \rangle$ for droplets and $\langle H \rangle = 1/2\langle r \rangle$ for cylindrical structures, we know from FFEM that $\langle H \rangle = 0$ for $\bar{T}$. Slight deviations in temperature or from an exactly spherical shape

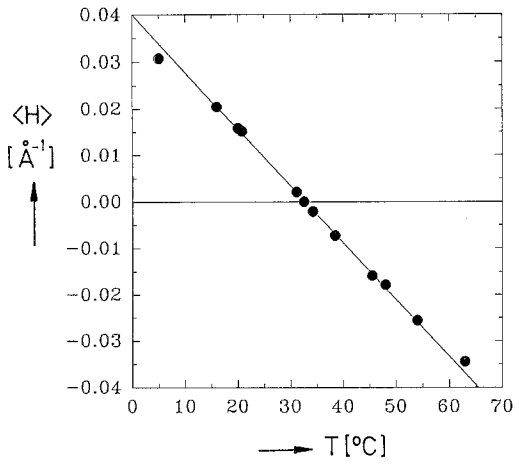

Fig. 10. Mean curvature as obtained from SANS and FFEM for the H_2O–n-octane–$C_{12}E_5$ system. Note the nearly linear variation around $\bar{T} = 32.6\,°C$ and change of sign there.

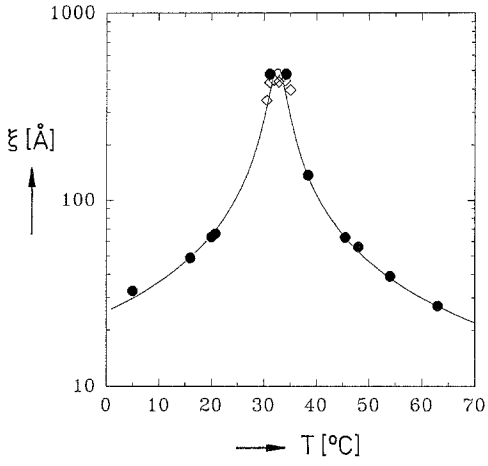

Fig. 11. Variation of characteristic length scale with temperature. Full line from Eq. (5).

are unimportant for the overall trends. The full line in Fig. 10 is calculated from

$$\langle H\rangle = 1.22\cdot 10^{-3}(\bar{T} - T)\,\text{Å}^{-1}\,, \tag{4a}$$

where $\bar{T} = 32.6\,°C$ and, approximately,

$$c_1 = 1.22\cdot 10^{-3}(T_u - T)\,\text{Å}^{-1}\,, \tag{4b}$$

and

$$c_2 = 1.22\cdot 10^{-3}(T_l - T)\,\text{Å}^{-1}\,. \tag{4c}$$

Obviously, the linear relation (Eq. (4a)) approximates the experimental data over a wide temperature range sufficiently well. The linear response of the observed interfacial curvature to the tuning of the parameter temperature suggests that a bending energy dictating the state of curvature has to be operative. Qualitatively, two well-known effects support the observed curving tendency of the surfactant film. Firstly, the hydration of the head groups decreases and, secondly, the oil penetration into the tails of the surfactant increases with increasing temperature. Both effects therefore would explain the inversion from oil-in-water to water-in-oil structures.

Mean domain size

The mean curvature, defined by the principal curvatures, goes through zero at $\bar{T}$. The mean domain size reaches its maximum there, but does not diverge. Thus, simply assuming $\xi = 1/\langle H\rangle$ does not suffice. Rather, one could define a mean characteristic length ξ in the system empirically as

$$\xi^{-2} = \tfrac{1}{2}[c_1^2 + c_2^2]\,. \tag{5}$$

Interestingly, Eq. (5) fits equally well the droplet regime where $\xi = 1/H$ and the bicontinuous regime where $\xi = 6\frac{v_s}{a_s}\frac{\phi_o\phi_w}{\phi_s}$ is a sufficient description [53]. Several experimental scattering investigations seem to indicate that ξ may be approximated by $\xi \approx \frac{d}{2}$ with d being the periodicity obtained from the maximum of ubiquitous scattering peak [54]. In Fig. 11, we show how well the experimental data points agree with the theoretical curve calculated from Eq. (5) where the open symbols stem from bicontinuous peaks. The full points correspond to the droplet radii except for the two highest ones which stem from tubular structures ($\xi = 1/2\langle H\rangle$) investigated in film contrast near T_l and T_u, respectively.

Interfacial tension and bending elasticity

The most striking feature of systems driven through phase inversion is the extreme minimum of interfacial tension either between the microemulsion and the excess phase or, in the three-phase regime, the tension between water- and oil-rich excess phase, where it can be measured by

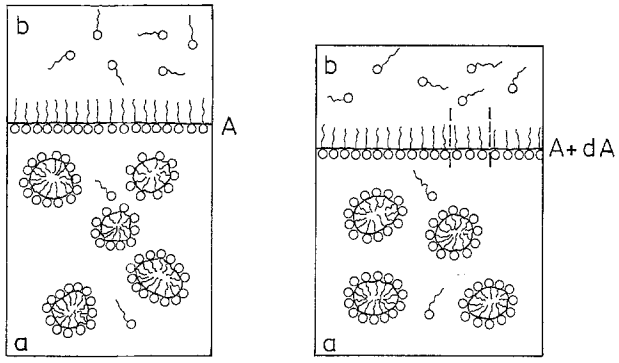

Fig. 12. Schematic illustration of interfacial tension experiment: Upon an increase of the bulk interfacial area A by dA, the area is filled in by interfacial film supplied by the microemulsion droplets, which have to be unbent. As a result, interfacial tension experiments, at least in part, measure "bending energy".

removing the middle phase. Interestingly, the characteristic functional form appears to be similar irrespective of the particular system [59, 66–72]. Depending on the strength of the surfactant the interfacial tension is reduced by several orders of magnitude near the three-phase state. The minimum is always observed when the bicontinuous microemulsion takes up equal volumes of water and oil. Sometimes interfacial tensions as low as 10^{-4} mN/m have been reported. For this reason the tensions are often referred to as ultra-low [59]. We will argue that from the definition of interfacial tension it follows that interfacial tension measurements are actually experiments sensitive to the bending properties of the interfacial films involved. For that purpose, consider Fig. 12, a schematic diagram illustrating the principal argument. Interfacial tension

$$\sigma_{ab} = \left[\frac{\partial F}{\partial A}\right]_{n_i, T, V} . \tag{6}$$

is the change in free energy F of the closed system upon an infinitesimal increase of the contact area A of the two bulk phases. Considering, for example, the closed system in Fig. 12, corresponding to a water-rich microemulsion in contact with excess oil (that is, $\underline{2}$ in Fig. 1) as we change the shape of the container maintaining its volume constant, the macroscopic amphiphile loaden interface will increase by dA. In order to prevent direct water/oil contact, microemulsion droplets will supply interfacial film, while their oil content at the same time becomes part of the bulk oil excess phase. The monomer concentration of amphiphilic molecules in the bulk phases will remain constant because they are saturated. Accordingly, in this process amphiphilic film becomes part of the macroscopic interface, having there a different curvature than in the microemulsion. There it has become flat on average, while it was bent before shaping the microemulsion droplet interface. Part of the free energy price to be paid is therefore the difference in bending energy before and after the tension experiment. In spinning drop experiments, one routinely carries out such an area increase of the bulk drop injected while the system is maintained at constant temperature and volume. The free energy per unit area associated with curvature deformations is accounted for by the Helfrich form [19]

$$f = 2\kappa(H - c_0)^2 + \bar{\kappa} c_1 c_2 , \tag{7}$$

where c_0 is the spontaneous curvature. Safran [60] has shown that for spheres (where $H = c_1 = c_2$), minimizing the bending free energy in Eq. (7) ($df/dH = 0$), one obtains the equilibrium sphere size. This permits to express the spontaneous curvature by the experimentally observable curvature H

$$c_0 = H\left(1 + \frac{\bar{\kappa}}{2\kappa}\right) . \tag{8}$$

Equation (8) predicts that the bending energy of a droplet microemulsion is minimized by a trade-off between the two stress components in Eq. (7) stemming from curvature and saddle-splay deformations, respectively. In deriving Eq. (8) entropy of dispersion or fluctuations and interactions of the droplets have been neglected. These effects are discussed in the Appendix. The bending energy in the two occurring states reads for the bent state in the microemulsion denoted by index (m),

$$f_b^m = 2\kappa(H^2 - 2Hc_0 + c_0^2) + \bar{\kappa} c_1 c_2 , \tag{9}$$

and for the flat one in the macroscopic interface (∞), where $c_1 = c_2 = H = 0$,

$$f_b^\infty = 2\kappa c_0^2 . \tag{10}$$

In order to investigate which part of the free energy change stems from the bending energy, we

now assume the free energy of the system to be determined solely by the bending energy of the film

$$F = A_m f_b^m + A_\infty f_b^\infty \,. \tag{11}$$

We further assume that the number of surfactant molecules which are dissolved as monomers in the bulk phases remains constant during the interfacial tension experiment. The residual surfactant molecules then shape the interfacial film either in the microemulsion with area A_m or in the flat macroscopic interface with area A_∞. For the free energy difference monitored in the interfacial tension experiments, we obtain

$$dF = F^{(1)} - F^{(2)} = (A_m^{(1)} - A_m^{(2)}) f_b^m + (A_\infty^{(1)} - A_\infty^{(2)}) f_b^\infty \,. \tag{12}$$

Observing that the microemulsion interfacial area decreases by the same amount by which the macroscopic interface increases, we have

$$dA = -(A_m^{(1)} - A_m^{(2)}) = A_\infty^{(1)} - A_\infty^{(2)} \,. \tag{13}$$

The experimentally measured interfacial tension then becomes

$$\sigma_{ab} = \frac{dF}{dA} = -f_b^m + f_b^\infty \,. \tag{14}$$

Inserting Eq. (9) and (10) and eliminating c_0, therein using Eq. (8) (also for the narrow intermediate range of bicontinuous structures, where the exact form for c_0 does not matter, because $H \to 0$ and $c_0 \to 0$), we obtain

$$\sigma_{ab} = 2H^2(\kappa + \bar{\kappa}) - \bar{\kappa} c_1 c_2 \tag{15}$$

for the interfacial tension. In Fig. 13, we show the interfacial tensions as function of temperature for the same system for which the domain sizes and curvatures were determined above. It shows the characteristic minimum typical for Winsor systems [59, 66–72]. Since the principal curvatures are known as function of temperature the two parameters κ and $\bar{\kappa}$ can be determined assuming them to be temperature independent in order to not complicate this first analysis. The minimum of the interfacial tension at $\bar{T}$, where the first term in Eq. (9) vanishes, determines the absolute value and, in particular, the positive sign of $\bar{\kappa}$, because $K = c_1 c_2$ is negative, but σ_{ab} is positive. The full

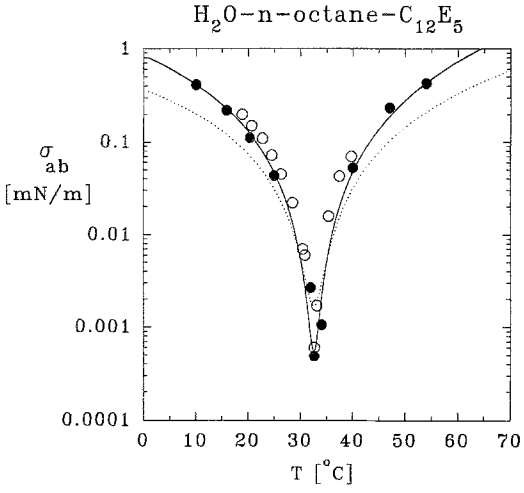

Fig. 13. Interfacial tension of interface between bulk oil-rich (a) and water-rich (b) phase in the H_2O–n-octane–$C_{12}E_5$ system measured with spinning drop (full symbols). The full line is calculated from Eq. (15) using the elastic moduli given in the text. For comparison the open symbols measured by laser light scattering [83] are shown (open symbols). The dashed line indicates a possible contribution of entropy of dispersion according to Eq. (A9).

line in Fig. 13 is calculated from Eq. (15) using Eqs. (1) and (4). The only free parameters are the bending modulus $\kappa = 0.6kT$ and for the saddle-splay modulus $\bar{\kappa} = 0.3kT$. The actual values are quite precisely fixed. While the functional form of Eq. (15) exactly reproduces the peculiar shape of the interfacial tension-temperature curve, the obtained value for κ is of the order of kT, a value in the vicinity of values determined by other techniques for related systems [59]. Furthermore, the value of $\bar{\kappa}$ is rather small so that according to Eq. (8) the radii of curvature experimentally observed and the calculated spontaneous curvature are close to each other on the phase boundary that has been termed emulsification failure boundary [60]. The determination of the bending moduli in this way is an interesting alternative, because interfacial tensions and microemulsion sizes are rather easy to determine experimentally. However, further quantitative experiments are needed to carefully check the validity of the assumptions made. In particular, the influence of entropy of dispersion and renormalization require consideration.

As discussed in the Appendix, including an entropy contribution changes the values to

$\kappa = 0.8kT$ and $\bar{\kappa} = -0.8kT$, respectively. Simply the inclusion of the ideal entropy of mixing thus leads to a change of sign for $\bar{\kappa}$, negative values being expected from interfacial stress profile calculations. Also, the condition $\bar{\kappa}/\kappa > -2$ for stability of Eq. (9) is fulfilled, as discussed by Safran in [60]. In Fig. 13 we show as dashed line the entropy contribution (Eq. (A9)). Clearly, examining interfacial tensions "as if curvature and bending energy were not a factor", as Kahlweit and Reiss [79] put it, is insufficient to explain the peculiar shape of the interfacial tension curves. Rather, both bending energy and entropy contributions (and possibly others) should be considered.

Furthermore, one might argue that the bending moduli appearing in Eq. (15) are renormalized values (see Appendix, [81]). Assuming this, the fit of Eq. (15) results in values for the bare moduli of $\kappa_0 = 1.4$ and $\bar{\kappa}_0 = -1.8kT$. It is interesting to note that inclusion of further contributions, that is, taking, for example, Eq. (A10) instead of Eq. (15), results in theoretical curves indistinguishably close to the full line in Fig. 13. The changes manifest themselves mainly in the specific figures for the bending moduli, as discussed. Experiments to further clarify the relative importance of the individual contributions are underway [83, 84].

It is appropriate to mention that the interconnection of bending energy and interfacial tension has previously been discussed [59, 68, 18, 85, 86]. However, here for the first time the application over the whole temperature range comprising Winsor I, II, and III has been performed, including the characterization of the occurring structures, domain sizes, and curvatures. The fact that the functional form of Eq. (15) is capable of describing the measured interfacial tension so well over the whole range with the aid of only two fitting parameters, suggests that the bending properties of the interfacial films are indeed the important properties determining the types of microstructures formed. Therefore, the assignment of importance to the bending properties by modern theories [73–78] in explaining phase behavior and microstructure seems to be justified. Furthermore, the notion of interfacial curvature as the determinant of microemulsion structures, as discussed for ionic microemulsions [82], is supported by the present study. An interpretation of the stability of microemulsions on the basis of macroscopic interfacial tensions alone, presented as an alternative to the bending energy approach [79, 80], in view of the above results, finds its natural explanation in the connection of interfacial tension *measurement* and bending energy as discussed above.

Conclusions

The fact that the phase behavior and associated microstructures of microemulsion systems are similar irrespective of the nature of the solvents and the amphiphiles, suggests that common phenomenological parameters govern these systems. Apparently, they vary systematically and do not differ very much from system to system. Previous authors have identified the interfacial curvatures, the spontaneous curvature, and two bending elastic constants as the relevant parameters (see, e.g., [59, 60]). From molecular theories it is evident that these parameters are interrelated through the interfacial stress profile. By clarifying systematic trends in the microstructures and extracting the characteristic domain sizes, we showed that bending energy alone would explain the interfacial tension measurements with bending moduli of order kT. Inclusion of entropy of dispersion has an influence on the specific numerical figures. Accordingly, further experiments are needed to clarify the open questions. While the analysis is not yet entirely rigorous, it constitutes a very strong plausibility argument that the inhomogeneous stress profile of the amphiphilic film simultaneously governs phase behavior, microstructure, and the ultra-low interfacial tensions observed.

Acknowledgement

Part of the work was performed in the department of Prof. M. Kahlweit. I wish to express my gratitude for his continuing support of and interest in the work. The SANS experiments were done in collaboration with L. Magid and B. Farago, while for the FFEM the expertise of W. Jahn was indispensable. Contributions by T. Sottmann and G. Busse in determining the interfacial properties are also gratefully acknowledged. I wish to thank S. Safran and D. Langevin for illuminating discussions; to the latter, I am particularly indebted for permission to use their unpublished data for comparison.

Appendix

An estimate of the free energy of dispersion may be obtained considering the ideal mixing entropy (for alternative discussions see, e.g., ref. [85, 86])

$$dF_{\text{mix}} = -Td(\Delta S_{\text{mix}}) \tag{A1}$$

with

$$\Delta S_{\text{mix}} = -Nk[x_1 \ln(x_1) + x_m \ln(x_m) + \cdots], \tag{A2}$$

where the total number of molecules is N. The mole-fraction of surfactant monomers and microemulsion droplets in the microemulsion phase are x_1 and x_m, respectively. Here, we have assumed that $x_i \ll 1$ valid for dilute systems. Above the CMC, x_1 is constant so that

$$d(\Delta S_{\text{mix}}) = -Nk dx_m(\ln(x_m) + 1), \tag{A3}$$

with

$$dx_m = -\frac{dA}{a_s N m}, \tag{A4}$$

and we have

$$\frac{dF_{\text{mix}}}{dA} = -\frac{kT}{a_s m}(\ln(x_m) + 1). \tag{A5}$$

Observing that the aggregation number m is given by

$$m = \frac{4\pi\xi^2}{a_s}, \tag{A6}$$

and that

$$x_m = \frac{x - x_1}{m}, \tag{A7}$$

Eq. (A5) reads

$$\frac{dF_{\text{mix}}}{dA} = -\frac{kT}{4\pi\xi^2}\left[\ln\left(\frac{x - x_1}{4\pi\xi^2} a_s\right) + 1\right]. \tag{A8}$$

That is, in sufficient approximation for the experiments considered, we have

$$f_{\text{mix}} = +\frac{kT}{2\pi\xi^2} \ln\left(\frac{\xi}{c}\right), \tag{A9}$$

where $c = 0.3\ (\pm 0.1)$ Å. Adding the entropy contribution from Eq. (A9) to Eq. (15), one has

$$\sigma_{ab} = 2H^2(\kappa + \bar{\kappa}) - \bar{\kappa} c_1 c_2 + \frac{kT}{2\pi\xi^2} \ln\left(\frac{\xi}{c}\right). \tag{A10}$$

The fit parameters for the bending moduli change accordingly, $\kappa = 0.8kT$ and $\bar{\kappa} = -0.8kT$, where the sign of $\bar{\kappa}$ has become negative. The individual contribution by Eq. (A9) is shown as a dashed line in Fig. 13. The application of Eq. (A9) over the whole temperature range includes the narrow range between 31 ° and 34 °C where the bicontinuous structure is present. For bicontinuous structures the mixing entropy can be estimated in random mixing approximation [60] leading to very similar values for the entropy of mixing. Converting the free energy contribution per unit volume (Eq. (2) in ref. [78]) into free energy per unit area, one has

$$f_{\text{mix}}^{\text{bicont}} = -\frac{kT}{6\xi^2\phi(1-\phi)} \times (\phi \ln\phi + (1-\phi)\ln(1-\phi)). \tag{A11}$$

For water oil symmetry at $\bar{T}$, Eq. (A11) reduces to

$$f_{\text{mix}}^{\text{bicont}} = 0.46\frac{kT}{\xi^2}, \tag{A12}$$

differing from Eq. (A9) by a factor of 2, which in view of the open questions and the assumptions made is a sufficient agreement. Thus it appears, for the time being and with the possible inaccuracy in mind, reasonable to apply Eq. (A9) also for the intermediate, bicontinuous range.

Further, one might ask for the effect of renormalization, that is, to account the lengthscale dependence of the bending moduli. Discussing this effect, we follow Golubovic and Lubensky [81], who obtained

$$\kappa = \kappa_0 - \frac{3kT}{4\pi} \ln\left(\frac{\xi}{a}\right) \tag{A13}$$

and

$$\bar{\kappa} = \bar{\kappa}_0 + \frac{10kT}{12\pi} \ln\left(\frac{\xi}{a}\right). \tag{A14}$$

Taking the renormalization in addition to the entropy of mixing into account results in fit parameters $\kappa_0 = 1.4kT$ and $\bar{\kappa} = -1.8kT$. These

observations are remarkable insofar as the changes in the parameters observed are all of the order of kT or less, so that precise experiments are needed to disentangle the individual contributions.

References

1. Bowcott JE, Schulman JH (1955) Z Elektrochem 59:283
2. Winsor PA (1954) Solvent Properties of Amphiphilic Compounds, Butterworth, London
3. Prince LM (1977) Microemulsions, Academic Press, New York
4. Bakker G (1928) Handbuch der Experimentalphysik, Akademische Verlagsanstalt, Leipzig, Vol. 6
5. Rowlinson JS, Widom B (1982) Molecular Theory of Capillarity, Clarendon, Oxford
6. Helfrich W (1981) In: Balinan R et al. (eds) "Physics of Defects", North-Holland, Amsterdam
7. Mitchell DJ, Ninham BW (1981) J Chem Soc Faraday Trans II 22:601
8. Petrov AG, Bivas I (1984) Prog Surf Sci 16:389
9. Lekkerkerker HNW (1989) Physica A 159:319
10. Lekkerkerker HNW (1990) Physica A 167:384
11. Winterhalter N, Helfrich W (1992) J Phys Chem 96:327
12. Gompper G, Zschokke S (1991) Europhys Lett 16:731
13. Bensimon D, David F, Leibler S, Pumir A (1990) J Phys France 51:689
14. Szleifer I, Ben-Shaul A, Gelbart WM (1990) J Phys Chem 94:5081
15. Szleifer I, Kramer D, Ben-Shaul, Gelbart WM, Safran SA (1990) J Chem Phys 92:6800
16. Ennis J (1992) J Chem Phys 97:663
17. Markin VS, Kozlov MM, Leikin SL (1988) J Chem Soc Faraday Trans 2, 84:1149
18. Ljungren S, Eriksson JC (1992) Langmuir 8:1300
19. Helfrich W (1973) Z Naturforsch C 28:693
20. Evans E (1974) Biophys J 14:923
21. Miller CA, Hwan RN, Benton WJ, Fort T, Jr. (1977) J Colloid Interface Sci 61:554
22. Kaler EW, Davis HT, Scriven LE (1983) J Phys Chem 79:5685
23. Auvray L, Cotton JP, Ober R, Taupin C (1984) J Phys Chem 88:4586
24. Guest D, Auvray L, Langevin D (1985) J Phys Lett 46:L-1055
25. Pouchelon A, Meunier J, Langevin D, Chatenay D, Cazabat AM (1980) Chem Phys Lett 76:277
26. Bellocq AM, Biais J, Bothorel P, Clin B, Fourche G, Lalanne P, Lemaire B, Lemanceau B, Roux D (1984) Adv Colloid Interface Sci 20:167
27. van Niewkoop J, Snoei (1985) J Colloid Interface Sci 103:400
28. Guering P, Lindman B 1985 (1985) Langmuir 1:464
29. Robbins ML, Bock J (1988) J Colloid Interface Sci 124:462
30. de Bruyn PL, Overbeek JTG, Verhoeckx (1989) J Colloid Interface Sci 127:244
31. Saito H, Shinoda K (1967) J Colloid Interface Sci 24:10
32. Shinoda K (1967) In: Shinoda K (ed) Solvent Properties of Surfactant Solutions, Marcel Dekker, New York
33. Shinoda K, Saito H (1968) J Colloid Interface Sci 26:70
34. Shinoda K, Takeda H (1979) J Colloid Interface Sci 32:64
35. Shinoda K, Kunieda H (1973) J Colloid Interface Sci 42:381
36. Shinoda K, Friberg S (1975) Adv Colloid Interface Sci 4:281
37. Kunieda H, Shinoda K (1982) J Dispers Sci Techn 3:233
38. Kahlweit M, Strey R (1985) Angew Chem Int Ed 24:654
39. Kahlweit M, Strey R, Firman P (1986) J Phys Chem 90:671
40. Kahlweit M, Strey R, Haase D, Firman P (1988) Langmuir 4:785
41. Kahlweit M, Strey R, Firman P, Haase D, Jen J, Schomäcker R (1988) Langmuir 4:499
42. Kahlweit M, Strey R, Schomäcker R, Haase D (1989) Langmuir 5:305
43. Kahlweit M, Strey R, Busse G (1990) J Phys Chem 94:3881
44. Kahlweit M, Strey R, Haase D, Kunieda H, Schmeling T, Faulhaber B, Borkovec M, Eicke HF, Busse G, Eggers F, Funck Th, Richmann H, Magid L, Söderman O, Stilbs P, Winkler J, Dittrich A, Jahn W (1987) J Colloid Interface Sci 118:436
45. Jahn W, Strey R (1987) In: Meunier J, Langevin D, Boccara N (eds) Physics of Amphiphilic Layers, Proceedings in Physics, Springer, Berlin, Vol 21, p 353
46. Jahn W, Strey R (1988) J Phys Chem 92:2294
47. Strey R (1992) Habilitation Thesis, University Göttingen
48. Friberg S, Kunieda H (1981) Bull Chem Soc Jpn 54:1010
49. Bodet JF, Bellare JR, Davis HT, Scriven LE, Miller WG (1988) J Phys Chem 92:1898
50. Vinson PK, Sheehan JG, Miller WG, Scriven LE, Davis HT (1991) J Phys Chem 95:2546
51. Kegel WK, Lekkerkerker HNW (1993) J Phys Chem 97:11124
52. Strey R, Winkler J, Magid L (1991) J Phys Chem 95:7502
53. Lichterfeld F, Schmeling T, Strey R (1986) J Phys Chem 90:5762
54. Teubner M, Strey R (1987) J Chem Phys 87:3195
55. Olsson U, Nagai K, Wennerström H (1988) J Phys Chem 92:6675
56. Strey R, Magid L, Farago B (1990) unpublished results
57. Farago B (1992) In: Chen SH et al (eds) Structure and Dynamics of Strongly Interacting Colloids and Supramolecular Aggregates in Solution, Kluwer, p 365
58. Farago B, Strey R, Magid L (1994) in preparation
59. Langevin D (1992) In: Chen SH et al (eds) Structure and Dynamics of Strongly Interacting Colloids and Supramolecular Aggregates in Solution, Kluwer, p 325
60. Safran SA (1992) In: Chen SH et al (eds) Structure and Dynamics of Strongly Interacting Colloids and Supramolecular Aggregates in Solution, Kluwer, p 237
61. Salager JL, Minana-Perez M, Perez-Sanchez M, Ramirez-Gouveia M, Rojas CI (1983) J Disp Sci Techn 4:313
62. Eicke HF, Shepherd JCW, Steinmann A (1976) J Colloid Interface Sci 56:168
63. Eicke HF (1982) In: Robb ID (ed) Microemulsions, Plenum Press, New York, p 17

64. Eicke HF, Hilfiker R, Holz M (1984) Helv Chim Acta 67:361
65. Boned C, Peyrelasse J (1991) J Surface Sci Technol 7:11
66. Wade WH, Morgan JC, Schechter RS, Jacobson JK, Salager JL (August 1978) SPE Journal 242
67. Kunieda H, Friberg S (1982) Bull Chem Soc Jpn 55:1777
68. Aveyard R, Binks BP, Fletcher PDI (1990) In: The Structure, Dynamics and Equilibrium Properties of Colloidal Systems, Kluwer, p 557
69. Aveyard R, Binks BP, Clark S, Mead J (1986) J Chem Soc Faraday Trans 1, 82:125
70. Seeto Y, Puig JE, Scriven LE, Davis HT (1983) J Colloid Interface Sci 96:360
71. Pouchelon A, Meunier J, Langevin D, Chatenay D, Cazabat AM (1980) Chem Phys Lett 76:277
72. Bonkhoff K, Hirtz A, Findenegg GH (1991) Physica A 172:174
73. Safran SA, Roux D, Cates M, Andelman D (1986) Phys Rev Lett 57:491
74. Milner ST, Safran SA, Cates ME, Andelman D, Roux D (1988) J Phys France 9:1065
75. Cates ME, Roux D, Andelman D, Milner ST, Safran SA (1988) Europhys Lett 5:733
76. Borkovec M (1989) J Chem Phys 91:6268
77. Borkovec M (1992) Adv Colloid Interface Sci 37:195
78. Cates ME, Andelman D, Safran SA, Roux D (1988) Langmuir 4:802
79. Kahlweit M, Reiss H (1991) Langmuir 7:2928
80. Kahlweit M, Jen J, Busse G (1992) J Chem Phys 97:6917
81. Golubovic L, Lubensky TC (1990) Phys Rev A41:4343
82. Chen SJ, Evans DJ, Ninham BW, Mitchell DJ, Blum FD, Pickup S (1986) J Phys Chem 90:842
83. Sicoli F (1993) Thesis, University of Paris and to be published (with D. Langevin)
84. Strey R, Sottmann T, work in progress
85. Overbeek GTH, Verhoeckx GJ, de Bruyn PL, Lekkerkerker HNW (1987) J Colloid Interface Sci 119:422
86. Israelachvili J (1987) In: Mittal KL and Bothorel P (eds) Surfactants in Solution, Plenum, p. 3

Received August 26, 1993;
accepted November 5, 1993

Author's address:

Dr. R. Strey
Max-Planck-Institut für Biophysikalische Chemie
Postfach 2841
37018 Göttingen, Germany